Novel electrochemiluminescent assay for the aptamer-based detection of testosterone

Rocío Cánovas,[‡,a,b] Elise Daems,[‡,a,b,c] Rui Campos,[‡,a,b] Sofie Schellinck,[d] Annemieke Madder,[e] José C. Martins,[d] Frank Sobott,[c,f,g] Karolien De Wael*[,a,b]

[a] A-Sense Lab, Department of Bioscience Engineering, University of Antwerp, Groenenborgerlaan 171, 2020 Antwerp, Belgium.

[b] NANOlab Center of Excellence, University of Antwerp, Groenenborgerlaan 171, 2020 Antwerp, Belgium.

[c] BAMS Research Group, Department of Chemistry, University of Antwerp, Groenenborgerlaan 171, 2020 Antwerp, Belgium.

[d] NMR and Structure Analysis Research Group, Department of Organic and Macromolecular Chemistry, Ghent University, Ghent 9000, Belgium.

[e] Organic and Biomimetic Chemistry Research Group, Department of Organic and Macromolecular Chemistry, Ghent University, Ghent 9000, Belgium.

[f] Astbury Centre for Structural Molecular Biology, University of Leeds, Leeds LS2 9JT, UK.

[g] School of Molecular and Cellular Biology, University of Leeds, Leeds, LS2 9JT, UK.

[‡] Sharing first authorship

*** Corresponding author:** Karolien De Wael (karolien.dewael@uantwerpen.be)

Abstract

This work presents a proof-of-concept assay for the detection and quantification of small molecules based on aptamer recognition and electrochemiluminescence (ECL) readout. The testosterone-binding (TESS.1) aptamer was used to demonstrate the novel methodology. Upon binding of the target, the TESS.1 aptamer is released from its complementary capture probe – previously immobilized at the surface of the electrode – producing a decrease in the ECL signal after a washing step removing the released (labeled) TESS.1 aptamer. The analytical capability of the ECL assay towards testosterone detection was investigated displaying a linear range from 0.39 to 1.56 µM with a limit of detection of 0.29 µM. The selectivity of the proposed assay was assessed by performing two different negative control experiments; *i)* detection of testosterone with a randomized ssDNA sequence and *ii)* detection of two other steroids, *i.e.* deoxycholic acid and hydrocortisone with the TESS.1 aptamer. In parallel, complementary analytical techniques were employed to confirm the suggested mechanism: *i)* native nano-electrospray ionization mass spectrometry (native nESI-MS) was used to determine the stoichiometry of the binding, and to characterize aptamer-target interactions; and, *ii)* isothermal titration calorimetry (ITC) was carried out to elucidate the dissociation constant (K_d) of the complex of testosterone and the TESS.1 aptamer. The combination of these techniques provided a complete understanding of the aptamer performance, the binding mechanism, affinity and selectivity. Furthermore, this important characterization carried out in parallel validates the real functionality of the aptamer (TESS.1) ensuring its use towards selective testosterone binding in further biosensors. This research will pave the way for the development of new aptamer-based assays coupled with ECL sensing for the detection of relevant small molecules.

Keywords: electrochemiluminescence, native nESI-MS, aptamer, small molecules, testosterone, dissociation constant.

Graphical abstract:

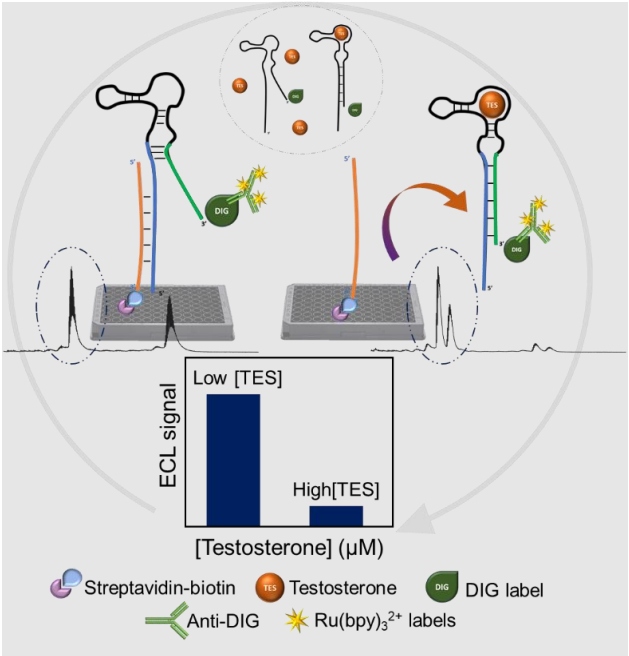

1. Introduction

Aptamers are synthetic single-stranded (ss) DNA or RNA oligonucleotides first described in 1990 after the development of the Systematic Evolution of Ligands by Exponential enrichment (SELEX) method and proposed to be a promising alternative to commercially available antibodies [1,2]. The greatest advantages of these oligonucleotide-based biorecognition elements with respect to their protein-based counterparts are: *i)* their high stability over a wide range of temperatures and pH-values; *ii)* the fact they are synthetically produced, eliminating the use of cell lines or animals as required for antibodies [3]; which means they are *iii)* more affordable; and *iv)* easy to modify [1]. Additionally, aptamers can recover their native conformation after re-annealing [4,5]. The three-dimensional structure of aptamers is necessary for and may be induced by, the binding with the target [6]. In fact, aptamers often experience significant conformational changes upon target binding, which offer great flexibility in the design of novel biosensors [4,7]. Signal moieties, *e.g.* fluorophores and quenchers, can be introduced to aid the detection [5], nevertheless, only a few aptamer-based sensors are currently commercialized and approved in diagnostics and therapeutics [1]. Besides, aptamers also show few disadvantages such as: *i)* susceptibility to nuclease degradation, *ii)* limited building block diversity, *iii)* PCR bias in SELEX method and *iv)* long aptameric sequences may interfere with the reproducibility and accuracy of the biosensors [1]. Another aspect that is important to mention is that the number of non-binding aptamers has been increasing showing that a multi-technique characterization is needed [8–10].

Aptamers have been reported for the recognition of numerous targets including proteins [11], peptides [12], enzymes [13,14], antibodies [15] and cell surface receptors [4], as well as small molecules [16] ranging from glucose and caffeine to steroids [17,18] and trinitrotoluene [19,20]. Small molecules are characterized by low molecular weight (<1000 Da) and often play an important role in regulatory biological pathways such as vitamins, hormones, messenger molecules and cofactors [6]. Nevertheless, the detection of these biomarkers is challenging due to their small size and often low concentrations (nanomolar range).

Nowadays, small molecules are commonly detected via chromatographic techniques, such as high-pressure liquid chromatography (HPLC) and gas chromatography (GC) coupled with mass spectrometry (MS) [1,6]. However, these methods often require a large amount of (more expensive) organic solvents, regular maintenance, trained personnel and a long-time of analysis. Therefore, the use of aptamer-based biosensors, with their potential high specificity, user-friendliness and a variety of different operational modes is a promising alternative for the detection and monitoring of small molecules [1].

In recent decades, electrochemical methods using aptamers as biological recognition elements have often been selected for the detection of various small molecules, such as neomycin B, aflatoxin B1, tetracycline, cocaine, bisphenol A, ochratoxin A, estradiol and dopamine [1,21,22]. However, electrochemiluminescence (ECL), a type of chemiluminescence reaction triggered by electrochemical methods, is gaining importance [4,23,24]. The combination of ECL with aptamers is so far mainly reserved

for large molecules such as proteins. For example, Duo and co-workers recently developed a slow off-rate modified aptamer (SOMAmer)-based approach using ECL for the quantification of a protein, glypican-3 [25]. Only a limited number of examples of aptamer-based electrodes for ECL analysis of small molecules can be found in the literature. **Table 1** summarizes the most common examples based on indium tin oxide, platinum, glassy carbon and screen-printed electrodes. The detection principle usually involves the use of luminophores such as a ruthenium-based complex, luminol-hydrogen peroxide-based reactions and/or quenchers. Noteworthy, all approaches are based on single or, in one case, dual-electrode systems [26] while none of them are capable of measuring several targets at the same time.

In general, the ECL technology ensures: *i)* the absence of a background optical signal; *ii)* the precise control of reaction kinetics offered by tuning the applied potential; *iii)* the compatibility with solution-phase and thin-film configurations; *iv)* the separation of excitation source (electronics) and detection readout (optical) which improves the sensitivity and *v)* the possibility to integrate nanomaterials (nanoparticles and nanotubes) to enhance the intensity of the signal [21].

Table 1. State of the art of ECL aptasensors for the single (or dual) detection of small molecules, linear range (LR) and limit of detection (LOD).

Electrode	Target	Detection method	Immobilization	Nanomaterials	LR	LOD	Ref.
ITO bipolar electrode	Adenosine	Oxidation of Fc labelled on adenosine aptamer with $Ru(bpy)_3^{2+}$/TPrA system.	via capture probe	no	1 fM – 0.10 µM	1 fM	[27]
ITO	Bisphenol A (BPA)	Release of the aptamer from capture probe upon addition of the target.	via capture probe	no	2 pM – 50 nM	1.5 pM	[28]
ITO	2,4,6-Trinitrotoluene (TNT)	In the presence of TNT, the aptamer–AuNPs would aggregate reducing the quenching effect, leading to ECL signal restoration.	Aptamer immobilized on AuNPs	AuNPs quenching the ECL emission of Ruthenium (II)	44 pM – 440 nM	16 pM	[29]
Platinum electrode	Kanamycin	Based on luminol-H_2O_2 properties in alkaline solution.	Aptamer immobilized on AgNPs	AgNPs as catalyzer for H_2O_2 decomposition	1 – 206 nM	0.12 nM	[30]
Platinum electrode	Kanamycin	Based on luminol-H_2O_2 properties + MWCNTs@TiO2/Thi.	Aptamer immobilized via Thi	MWCNTs@TiO_2 /Thi.	206 pM – 20.6 µM	101 pM	[31]
GCE	Bisphenol A	$Ru(bpy)_3^{2+}$ nanosheets luminophore and NCDs@PEI as co-reactant. ECL signal ↓ upon target binding.	Aptamer immobilized on AuNPs	Electrodeposited AuNPs	100 pM – 40 µM	33 pM	[32]
GCE	Ochratoxin A	CdS QDs quenched by Cy5. After target addition, Cy5-DNA is released from the electrode surface ↑ the ECL signal.	1) DNA walker complementary to aptamer + 2) Cy5-labeled ssDNA containing a 7-nucleotide nicking recog. sequence	no	0.05 – 5 nM	0.012 nM	[33]
GCE	Zearalenone	NH_2-Ru@ SiO_2 NPs and NGQDs ECL signal ↓upon binding of the target.	Aptamer immobilized on NGQDs-NH_2-Ru@SiO_2	NH2-Ru@ SiO_2 NPs	31 fM – 31 pM	3.14 fM	[34]
GCE	Ractopamine	(Ru@SiO_2 NPs) + AuNPs. The ECL signal is quenched by	Aptamer immobilized by Au-S bond on the	AuNPs as a catalyzer to redox reaction	1.5 pM – 15 pM	41 fM	[35]

		the energy transfer from luminophore to benzoquinone.	modified electrode surface				
SPCE	Malachite green and CAP	Dual detection using quenchers. Upon target recognition, the aptamer leaves and the ECL signal ↑.	via capture probe for each target in each WE	CdS quantum dots WE1 and luminol-gold NPs WE2	0.1–100 nM and 0.2–150 nM	0.03 nM and 0.07 nM	[26]
96-well plate (carbon)	Testosterone	Release of the aptamer from capture probe upon addition of the target (↓ ECL).	via capture probe	no	0.39 – 1.56 µM	0.29 µM	**This work**

ITO: indium tin oxide, $Ru(bpy)_3^{2+}$: tris(2,2'-bipyridyl)ruthenium(II); Fc: ferrocene; TPrA: tripropylamine; AuNPs: gold nanoparticles; AgNPs: silver nanoparticles; H_2O_2: hydrogen peroxide; MWCNTs: multiwall carbon nanotubes; TiO_2/Thi: titanium dioxide/thionine; BSA: bovine serum albumin; GCE: glassy carbon electrode; NCDs@PEI: poly(ethylenimine) functionalized nitrogen-doped carbon nanodots; CdS QDs: Cadmium sulfide quantum dots; NH_2-Ru@SiO_2 NPs: Amine-functionalized $Ru(bpy)_3^{2+}$-doped silica nanoparticles; NGQDs: nitrogen doped graphene quantum dots; CAP: Chloramphenicol; WE: working electrode.

In this manuscript, to the best of our knowledge, an aptamer-based assay system with capacity for the simultaneous ECL-based detection of multiple small molecules is presented for the first time. More specifically, we present a proof-of-concept ECL assay for the high-affinity detection of testosterone by the TESS.1 aptamer. Moreover, the aptamer performance, the binding mechanism, affinity and selectivity are unraveled thanks to the combination of analytical techniques such as isothermal titration calorimetry (ITC) [36] and native nano-electrospray ionization mass spectrometry (native nESI-MS) [37].

First, the analytical performance of the aptamer-based ECL assay towards testosterone detection is studied. Second, different negative control experiments are carried out by testing the interaction of testosterone with a randomized ssDNA sequence and by investigating two other steroids, *i.e.* deoxycholic acid and hydrocortisone with the TESS.1 aptamer. In parallel, *i)* native nESI-MS experiments are performed to determine the stoichiometry of binding, and for the identification and characterization of species; and, *ii)* ITC is used to elucidate the dissociation constant (K_d) of the TESS.1 aptamer for testosterone. This unique approach opens new perspectives and insights in the use of aptamers coupled with ECL sensing for the accurate and highly sensitive detection of a wide range of small molecules simultaneously.

2. Material and Methods

Detailed information related to the incubation protocol and complementary analytical techniques utilized along this work can be found in the supplementary material (SM).

2.1. Reagents

Sodium chloride and magnesium chloride were acquired from Fisher Scientific; potassium chloride and deoxycholic acid (98.5%) were purchased from Acros Organics (Thermo Fischer, USA); sodium phosphate dibasic, sodium phosphate monobasic, potassium phosphate dibasic and potassium phosphate monobasic salts, Tween 20 and testosterone (≥99.0%) were purchased from Sigma-Aldrich (Merck, USA); and hydrocortisone (>98.0%) from TCI (Tokyo Chemical Industries, Japan).

The stocks of testosterone (50 mM), deoxycholic acid (50 mM) and hydrocortisone (30 mM) were prepared in absolute ethanol (≥99.8%, from Fisher Scientific, USA) in DNA LoBind® Eppendorfs. The required dilutions of the target were performed using a hybridization buffer. Other solutions and buffers were prepared in ultrapure water (18.2 MΩ cm^{-1} double deionized water, Sartorius Arium® Ultrapure Water Systems). The pH was measured using a 913 pH meter from Metrohm (The Netherlands).

A hybridization buffer containing 10 mM phosphate buffer, 150 mM sodium chloride and 100 mM magnesium chloride and a washing buffer (PBS-T) with 137 mM sodium chloride, 2.7 mM potassium chloride, 10 mM sodium phosphate dibasic, 1.8 mM potassium phosphate monobasic and 0.05% v/v of Tween 20 were prepared in ultrapure water. The pH was adjusted to 7.0 by using a 1 M HCl or KOH solution.

2.2. DNA sequences

All DNA sequences were purchased from Eurogentec (Belgium). The randomized DNA sequence was derived from the TESS.1 aptamer and designed using the OligoAnalyzer Tool of Integrated DNA Technologies. The melting temperatures between capture probe-stem 1 and stem 1-stem 2 were predicted with the same platform (OligoAnalyzer Tool). The part complementary to the capture probe was preserved while the other nucleotides of the TESS.1 aptamer were scrambled. Non-functionalized DNA sequences were used for the ITC and native nESI-MS experiments, while the oligonucleotides carried some functionalizations for the ECL experiments. An overview is provided in **Table 2**. The capture probe was ordered with a biotin modification at the 3' end, whereas the TESS.1 aptamer and the randomized sequence carry a digoxigenin (DIG) modification at their 3' end.

Table 2. DNA sequences utilized in this work.

	Sequence of oligonucleotides	Functionalization
Capture probe	5'- GTC GTC CCG AGA G -3'	Biotin-TEG on 3'
Aptamer TESS.1	5'- CTC TCG GGA CGA CGG GAT GTC CGG GGT ACG GTG GTT GCA GTT CGT CGT CCC -3'	DIG on 3'
Randomized TESS.1	5'- CTC TCG GGA CGA CTG ACG GGC ACT CAG TTG TGT TGG GGT CTC GCC CGG TGG -3'	DIG on 3'
Short version of TESS.1 (TESS.1short)	5'- GGG ATG TCC GGG GTA CGG TGG TTG CAG TTC -3'	-
Stem 1	5'- CTC TCG GGA CGA CGG G -3'	-
Stem 2	5'- TTC GTC GTC CC -3'	-

* The bases underlined in the randomized TESS.1 are those whose position is different when compared to the TESS.1 aptamer. The nucleotides from stems 1 and 2 in common with the aptamers are represented in blue and green, respectively. The capture probe is colored in orange to keep the same color code in the entire manuscript and figures. The molecular weights (in Da) of the sequences are: capture probe = 3975.6, TESS.1+DIG = 16468.0, TESS.1 = 15787.2, randomized TESS.1+DIG = 16468.0, randomized TESS.1 = 15787.2, TESS.1short = 9562.3, stem 1 = 4923.2, and stem 2 = 3259.2.

2.3 Native nano-electrospray ionization mass spectrometry (native nESI-MS)

Prior to native nESI-MS analysis, the aptamer and randomized DNA sequences were dialyzed into 300 mM aqueous ammonium acetate (pH 6.8) using Slide-a-

Lyzer Mini dialysis units with a molecular weight cut-off of 3.5 kDa (Thermo Fisher Scientific) to desalt the samples and to provide a volatile electrospray buffer of appropriate ionic strength. The capture probe, stem 1 and stem 2 were not dialyzed due to their low molecular weight (3975.6 Da, 4923.2 Da and 3259.2 Da, respectively). The concentrations of the dialyzed aptamers were verified using a Nanodrop2000 (Thermo Scientific). Extinction coefficients were calculated by the Nanodrop2000 software based on the oligonucleotide sequences. Samples with a final concentration of 10 µM oligonucleotides (in equimolar ratios) and a 10-fold excess of the target were prepared. The capture probe and aptamer were incubated for 30 minutes before adding the target and incubating the mixture for 30 minutes.

Native nESI-MS analyses were performed on a Synapt G2 HDMS Q-TOF instrument (Waters, Wilmslow, UK) in the positive ionization mode. Approximately 2-4 µL of the sample was introduced into the mass spectrometer, using nESI with gold-coated borosilicate glass tapered-tip capillaries made in-house. The instrument was carefully tuned to preserve the native structure and non-covalent interactions. The spray capillary voltage ranged between 1.2-1.6 kV, the sampling cone voltage was 20 V and the extractor cone voltage was 1 V. The trap and transfer collision energy were set at 5 V and 0 V, respectively and the trap DC bias was fixed at 40 V. The IMS wave velocity was set to 800 m/s and the IMS wave height to 35 V. Gas pressures were 2.57 mbar and $2.2 \cdot 10^{-3}$ mbar for the backing and source gas, respectively. All data were analyzed using MassLynx v4.2 (Waters). The abundance of all bound and unbound states was estimated based on the peak area of the peaks including salt adducts.

2.4. Electrochemiluminescence measurements

The ECL measurements were performed according to the following protocol: *i)* the 96-well plate was washed once with 150 µL PBS-T and tap dried; *ii)* 25 µL of the capture probe (200 nM) were incubated in the well for 1 hour (always sealing the plate to avoid evaporation, all incubations were performed in a shaker at 550 rpm and RT). Simultaneously, *iii)* 55 µL of the aptamer solution (400 nM) were mixed with 55 µL of the target (10 µM) or buffer solution (as a blank) in an Eppendorf and incubated for 1 hour (550 rpm and RT). *iv)* After the incubation, the solution was discarded from the plate by washing 3 times with PBS-T and tap dried. *v)* Subsequently, 50 µL of the mixture of aptamer and target/buffer was added to the well plate and incubated for 1 hour with shaking (550 rpm and RT). Then, *vi)* this mixture was discarded from the plate by washing 3 times with PBS-T and tap dried. For the ECL readout, *vii)* 25 µL of 0.5 µg mL^{-1} functionalized anti-DIG conjugated with $Ru(bpy)_3^{2+}$ labels were incubated for 1 hour with shaking (550 rpm and RT); *viii)* the solution was discarded from the plate by washing 3 times with PBS-T and tap dried; *ix)* 150 µL of MSD GOLD Read Buffer (R92TG-1) were added to each well; and, *x)* the ECL signal was read immediately in the Meso Scale Diagnostics device (see **Fig. S1** in SM).

After investigating the effect of the TESS.1 aptamer concentration on the ECL signal, 200 nM was chosen as the optimal concentration, and used in the subsequent experiments, since it shows the largest decrease (61%) in ECL signal upon addition of 5 µM of testosterone, compared to a blank (**Fig. S2**). Throughout the experiments,

8 different target concentrations were used between 25 and 0 µM using twofold serial dilutions.

Functionalized anti-DIG antibodies (Goat polyclonal anti-digoxigenin antibody, AbCam, ab76907) were conjugated with tris(2,2'-bipyridyl)ruthenium(II) ($Ru(bpy)_3^{2+}$) labels using the MSD Gold Sulfo-Tag NHS-Ester conjugation kit (Meso Scale Diagnostics, Cat. R31AA-1) [38] thanks to the reaction between the amine groups of the antibody with the ester on the $Ru(bpy)_3^{2+}$ labels. The antibody carries multiple $Ru(bpy)_3^{2+}$ labels which emit light upon electrochemical stimulation. The ECL measurements were performed in a MESO QuickPlex SQ 120 controlled by the Methodical Mind reader software. The plates used were MSD GOLD™ 96-well Small Spot Streptavidin SECTOR Plates (L45SA-1) with streptavidin-coated carbon electrodes in the bottom of each well.

3. Results and Discussions

Our ECL assay is based on the principle of competitive binding. An oligonucleotide sequence partially complementary to the TESS.1 aptamer, named capture probe in this manuscript, is labeled with biotin and immobilized on streptavidin-coated working electrodes (96-well plate). The TESS.1 aptamer carries a DIG label (**Fig. 1a**) on its 3' end which allows the binding of the $Ru(bpy)_3^{2+}$ modified anti-DIG antibody [39,40]. The $Ru(bpy)_3^{2+}$ labels emit light upon electrochemical stimulation and the signal is amplified by tripropylamine (TPrA) present in the reading buffer.

The approach used in this manuscript is similar to that developed by Yang and co-workers but with remarkable differences. In their work *i)* the TESS.1 aptamer is labeled with fluorescein (F) on its 5' end, *ii)* the partially complementary oligonucleotide sequence carries a fluorescence quencher (D) on its 3' end (**Fig. 1b**) and *iii)* neither the aptamer nor the capture probe are immobilized on a surface. Upon addition of the target (testosterone), there is a dissociation of the TESS.1 aptamer from its complementary strand due to the binding of the TESS.1 aptamer to testosterone, leading to an increase in the fluorescent signal [5].

Here, as in the work of Yang *et al*., only the TESS.1 aptamer that does not bind to testosterone stays hybridized with the capture probe (**Fig. 1c**). This occurs when a blank solution (not containing testosterone), or a solution containing a steroid with no affinity to the TESS.1 aptamer is added to the wells. In these cases, the aptamer remains attached to the capture probe via stem 1 (colored in blue in **Table 1** and **Fig. 1**) as no binding with the target takes place.

To prevent non-specific adsorption, and non-specific signal, washing steps are introduced after each incubation. More specifically, after incubation with anti-DIG (before recording the ECL signal), the washing step ensures the removal of aptamer that reacted with the target and of the anti-DIG antibody that could be non-specifically adsorbed on the well surface. Thus, the ECL signal only comes from DIG-labelled aptamers still immobilized on the well surface. Considering that the aptamer dehybridizes from the capture probe upon binding of testosterone, the aptamer will be washed away and, consequently, no interaction with the anti-DIG antibody will take

place. Therefore, the ECL signal decreases upon increasing the concentration of testosterone (**Fig. 1c**).

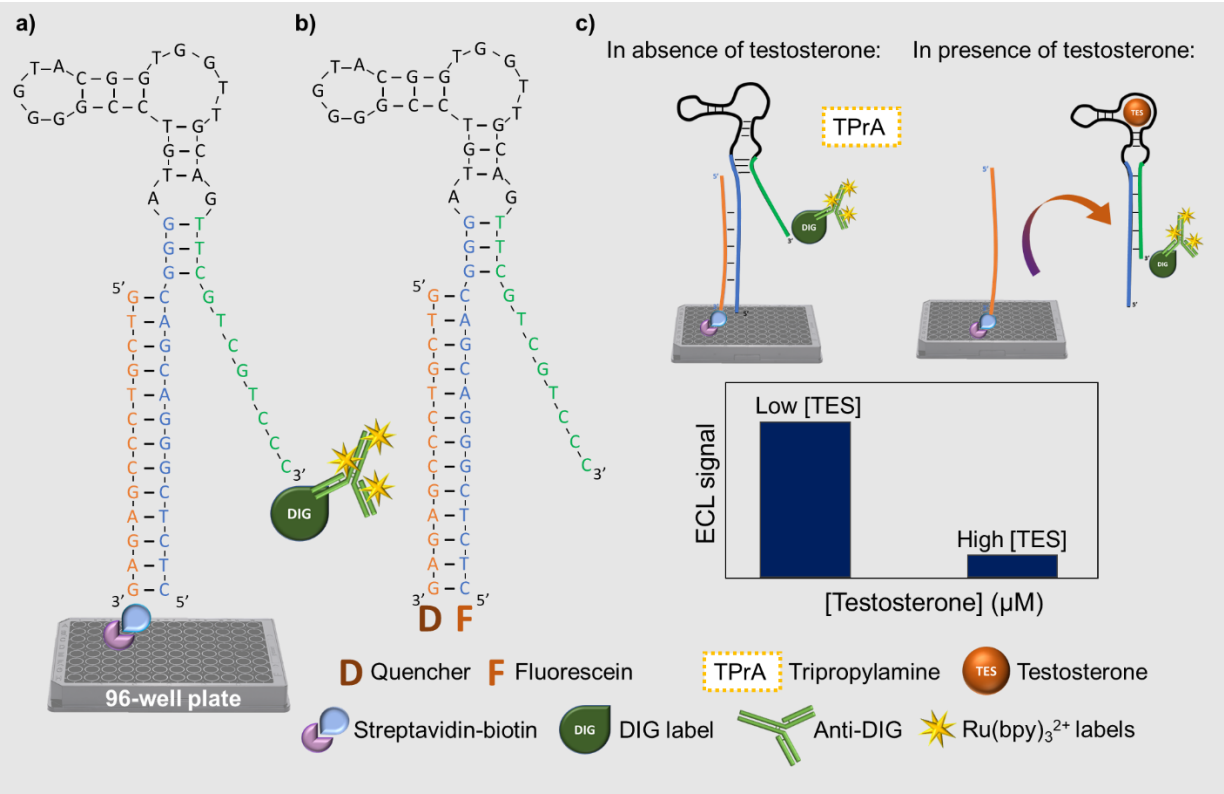

Fig. 1. Competitive binding principle. The TESS.1 aptamer used **a)** in the present work and **b)** by Yang *et al.* [5]. **c)** Schematic representation showing: on the left, the schematic hybridization between the capture probe (orange sequence attached to the 96-well plate) with the aptamer (stem 1 sequence, in blue) when the target is not present or at low concentrations; on the right, the aptamer dehybridizes from the capture probe after binding with the target (closing both stems); and the corresponding ECL signal produced after the addition of anti-DIG antibody with $Ru(bpy)_3^{2+}$ labels and TPrA (present in the reading buffer). The intensity of the ECL signal depends on the concentration of testosterone.

3.1. Characterization of the TESS.1 aptamer

The binding competent state of the TESS.1 aptamer implies a conformational change from a more unfolded conformation (without the target) to the folded structure (by closing both stems) when the target is present. Hence, stem 1 (in blue) and stem 2 (in green) will hybridize upon binding of the target, hampering stem 1 to interact with the capture probe in presence of testosterone (**Fig. 1c**). Firstly, to investigate whether stem 1 preferentially binds to the capture probe rather than to stem 2, native nESI-MS experiments with only the stems and capture probe were performed (**Fig. 2**).

When measuring a mixture of stem 1 (complementary to both capture probe and stem 2) and stem 2, a duplex of these stems is noticed (red dashed lines) and only low-intensity peaks for the stems alone (in blue and green) can be identified (**Fig. 2 – top**). The mixture of the capture probe and stem 1 also forms a duplex (**Fig. 2 – middle**, pink dashed lines). After combining all three species in an equimolar mixture, a clear signal for the capture-stem 1 duplex is observed while only a low-intensity peak for the stem 1-stem 2 duplex is detected (**Fig. 2 – bottom**). Thereby, native nESI-MS proved that the affinity of stem 1 to the capture probe is higher than that for stem 2. This is

based on the higher number of complementary base pairs (bp) between the capture probe-stem 1 (13 bp) in comparison with stem 1-stem 2 (9 bp) and their predicted melting temperatures of 56.1°C and 44.6°C, respectively.

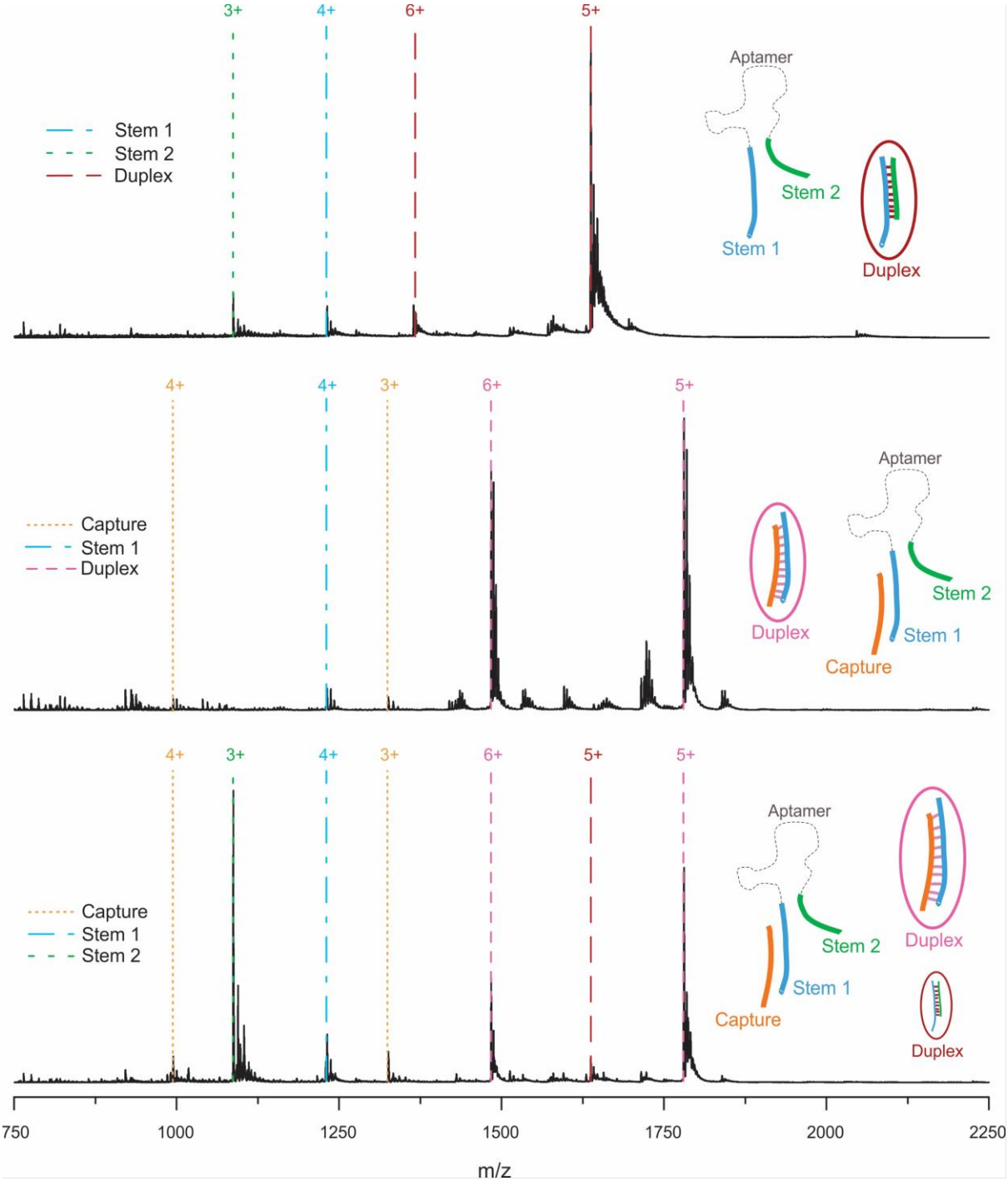

Fig. 2. Native nESI-MS spectra of stem 1 (complementary to the capture probe and stem 2) and stem 2 (complementary to the stem 1) **(top)**, capture probe and stem 1 **(middle)** and stem 1, stem 2 and the capture probe **(bottom)** in equimolar ratios. The lines represent the theoretical m/z-values for each species.

In the complete aptamer structure, stem 1 and stem 2 are, however, part of the same chain. This could result in some entropic advantage favoring the duplex formation of the stems instead of the hybridization of stem 1 and the capture probe. Therefore,

native nESI-MS experiments with the TESS.1 aptamer and capture probe were performed. The hypothesis was disproven as a clear signal for the aptamer (which contains stem 1) – capture complex is observed in the mass spectrum in the absence of testosterone (**Fig. 3 – top**, purple dashed lines). Simultaneously, there is some free aptamer (grey dashed lines) and free capture probe (orange dashed lines) detected. Importantly, some peaks are shifted to slightly higher m/z-values due to nonspecific binding of sodium ions, which are a common contamination in native nESI-MS. As previously mentioned, the proposed principle assumes that the aptamer cannot form a duplex with the capture probe upon binding to testosterone. Again, native nESI-MS was used to confirm this hypothesis. Upon addition of testosterone, the aptamer-capture probe interaction was almost completely disrupted and an aptamer-testosterone complex was formed closing stem 1 and stem 2 (**Fig. 3 – bottom**, green dashed lines).

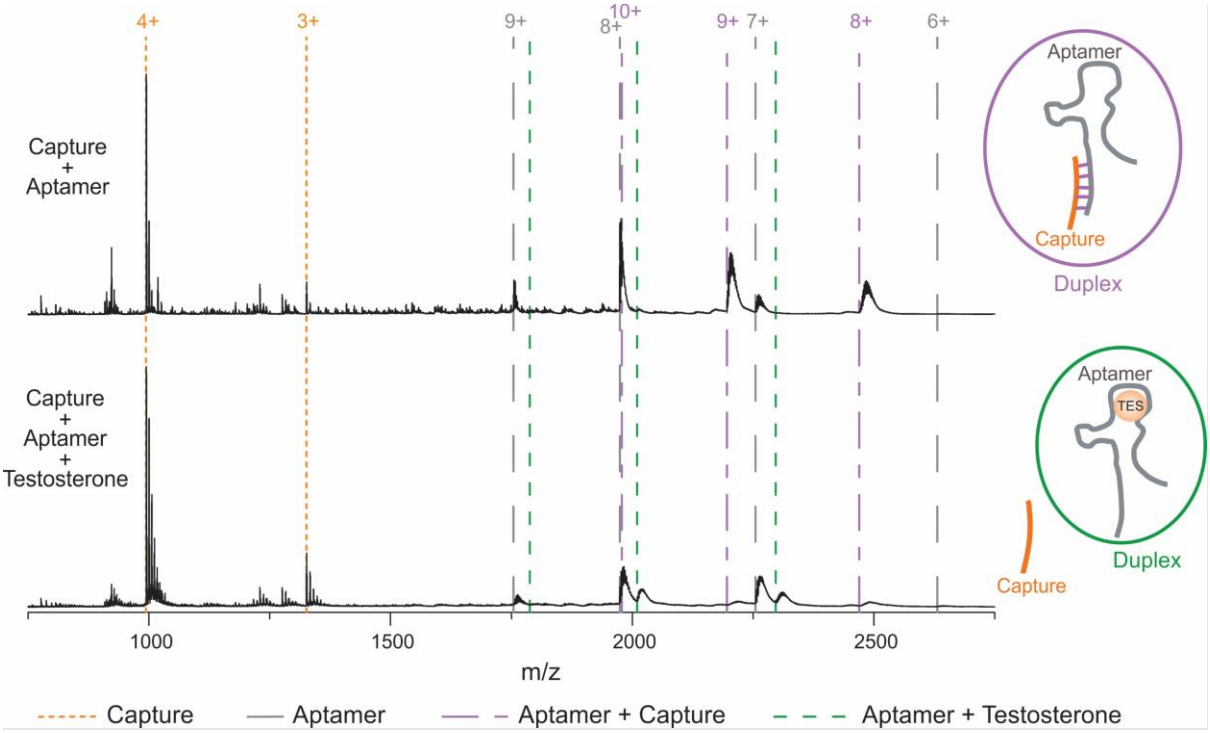

Fig. 3. Native nESI-MS spectrum of the aptamer and capture in a 1:1 ratio **(top)** and the same mixture with testosterone added in 10-fold excess **(bottom)**. The dotted orange lines, dashed grey lines, dotted green lines and dashed-dotted purple lines represent the theoretical m/z-values of the capture probe, aptamer, aptamer – testosterone complex and aptamer – capture probe complex, respectively.

To investigate whether the stems of the TESS.1 aptamer contribute to the binding affinity of testosterone, native nESI-MS experiments were performed with the full-length TESS.1 aptamer and a shorter variant, called TESS.1short, which is 21 nucleotides smaller. In this shorter aptamer, 13 nucleotides from stem 1 and 8 nucleotides stem 2 are removed. **Fig. S3a** displays the native nESI-MS spectrum of the full-length aptamer and **Fig. S3b** portrays the results acquired with the shorter version of the aptamer. A clear complex between the full-length TESS.1 aptamer and testosterone was identified as can be seen in **Fig. S3a**. In this case, 39% of the aptamer forms a complex with testosterone (see also **Fig. 4b**). On the other hand, the

TESS.1short aptamer only shows a low-intensity peak corresponding to the complex (13% of the aptamer is present as complex, green dashed lines in **Fig. S3b**).

ITC experiments were performed to determine the K_d between both the TESS.1 aptamer (**Fig. S4a**) and the TESS.1short (**Fig. S4c**) aptamer and testosterone. The thermograms show a clear exothermic binding process in both cases and the K_d was calculated to be 240 ± 29 nM (slightly higher than the previously reported value of ~80 nM by Yang *et al.* [5]) and 489 ± 58 nM, respectively (**Fig. S4c** and **S4d**). **Table S1** summarizes the parameters determined via ITC demonstrating slight differences between the TESS.1 and TESS.1short aptamers from a thermodynamic point of view, where the binding entropy of the TESS.1short aptamer is more negative than the TESS.1 aptamer, showing more unfavorable conformational changes and in consequence, less affinity [41].

These results suggest that even though the TESS.1short aptamer still contains the binding region, the stems of the TESS.1 aptamer are a crucial structural part for the folding of the aptamer into its binding-competent state, enhancing its affinity towards testosterone. Since stem 1 and stem 2 of the TESS.1 aptamer hybridize upon binding of the target, stem 1 is no longer available to interact with the capture probe, as shown in **Fig. 3**.

3.2. ECL detection of testosterone and native nESI-MS confirmation

TESS.1 aptamer. After the characterization of the TESS.1 aptamer, ECL experiments with multiple concentrations of testosterone were performed to gain a better insight into the binding of testosterone to its aptamer. **Fig. 4a** shows data of the TESS.1 aptamer in the presence of testosterone in a concentration range from 0 to 25 µM, showing a linear response from 0.39 to 1.56 µM with a limit of detection of 0.29 µM. This LOD was calculated following the formula LOD = 3.3(Sy/S), where Sy is the standard deviation of the blank (concentration of testosterone = 0 µM) and S is the slope obtained during the calibration curve (Table 1 and Table S2).

After the incubation of the aptamer with the different concentrations of testosterone, only the free aptamer (not bound to testosterone) will hybridize with the capture probe via the stem 1 of the aptamer and contribute to the recorded ECL signal. As can be noticed in the inset of **Fig. 4a**, the ECL signal already decreases 14% upon addition of the lowest concentration of testosterone used (0.39 µM). This decrease is due to the lower availability of the free TESS.1 aptamer to hybridize with the capture probe upon the addition of the target to the aptamer solution. The ECL response decreases up to 79% after the fourth addition of the target (3.13 µM), indicating that an increasing amount of testosterone is binding to TESS.1 aptamer in this range. From 3.13 µM onwards the signal is almost constant which suggests a saturation of the aptamer. A similar trend of the testosterone curve is observed in the results reported by Yang and co-workers where the fluorescent signal also reaches a plateau at concentrations above 3.13 µM [5]. **Fig. 4b** displays the native nESI-MS spectrum of the TESS.1 aptamer (grey dashed lines) and the complex formed with the target (green dashed lines), after the addition of the target in a 1:10 ratio, illustrating the efficient binding between TESS.1 aptamer and testosterone.

From the ECL experiments, the K_d was estimated using Chambers and Sauer [42] method, where the K_d equals the concentration of testosterone at which half-maximal binding of the TESS.1 aptamer occurs. Thus, the concentration of testosterone was found to be 970 nM. This is higher than the K_d determined by ITC, although it remains in the same range. It is important to consider that the presence of the capture probe (not present during ITC measurements) can likely influence the affinity by competing with the binding of testosterone.

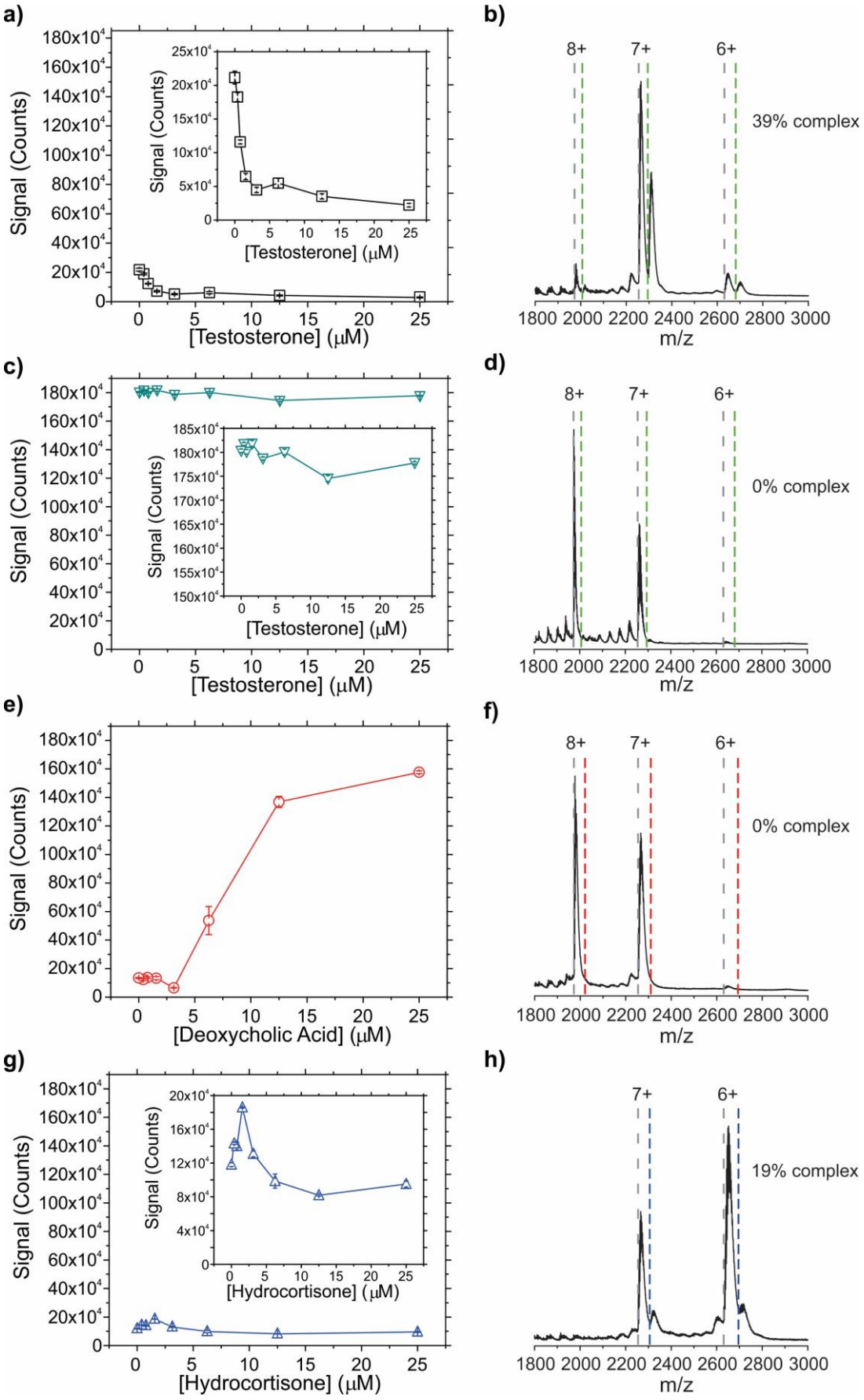

381 **Fig. 4**. On the left: ECL data of testosterone in combination with **a)** the TESS.1 aptamer and **c)**
382 randomized ssDNA sequence; and, ECL data of the negative controls **e)** deoxycholic acid and **g)**

hydrocortisone with the TESS.1 aptamer. Target concentrations ranged from 0 to 25 µM with a total of 8 concentrations in twofold dilutions. On the right, native nESI-MS spectra showing: **b)** TESS.1 aptamer and **d)** randomized DNA sequence after addition of testosterone (10-fold excess), **f)** TESS.1 aptamer after the deoxycholic acid addition (10-fold excess)and **h)** TESS.1 aptamer after the hydrocortisone addition (10-fold excess). Theoretical m/z-values of the aptamer and the random sequence are represented with a dashed grey line, whereas the aptamer-target complexes are represented with colored dotted lines (testosterone in green, deoxycholic acid in red and hydrocortisone in blue).

Specificity of the ECL approach: randomized ssDNA. To investigate whether the decrease in the signal can be ascribed to specific binding, the same experiments were performed using a randomized ssDNA sequence instead of the TESS.1 aptamer, as shown in **Fig. 4c**. It is important to highlight that the randomized sequence kept the part complementary to the capture probe to allow hybridization whereas the rest of the sequence was scrambled (see **Table 2** for more details). Native nESI-MS experiments with the randomized ssDNA were carried out to confirm and demonstrate that no binding occurs between this sequence and the target (see **Fig. 4d** in comparison with **Fig.4b**). In this case, the ECL signal at each concentration of testosterone is in the same range with a maximum deviation of 3% compared to the blank.

One thing that is important to notice is that the ECL signal of the randomized sequence (**Fig. 4c**) is much more intense than that of the TESS.1 aptamer (**Fig. 4a**). This is most likely due to the scrambled part that was designed to avoid self-complementarity within the TESS.1 aptamer. As a result, this unfolded structure of the randomized sequence promotes the position of the DIG label further away from the well surface, and therefore also the anti-DIG antibody with the $Ru(bpy)_3^{2+}$ labels with respect to the surface of the electrode. In consequence, the labels were closer to the light source during the generation and reading of the ECL signal, offering the highest values (~$180x10^4$ counts, **Fig. 4c**). The increase of the ECL response due to the larger distance between the ruthenium complex and the surface of the electrode has already been explained and demonstrated in the literature [43].

3.3. Selectivity of the TESS.1 aptamer and the developed ECL approach

Deoxycholic acid and hydrocortisone steroids were selected as negative controls to replace testosterone and confirm the selectivity of the TESS.1 aptamer. Hence, the native nESI-MS results showed no interactions between deoxycholic acid and the TESS.1 aptamer as can be seen in **Fig. 4f** (red dashed lines). In addition, only 19% of the complex between hydrocortisone and the TESS.1 aptamer was observed during the native nESI-MS experiments (**Fig. 4h**, blue dashed lines).

As depicted in **Fig. 4e**, in presence of deoxycholic acid the ECL signal becomes much more intense from 6.25 µM onwards to reach 10 times its initial value. The number of counts measured at 25 µM deoxycholic acid is in the same order of magnitude as the ECL signal observed for the unstructured randomized ssDNA (~$160x10^4$ and ~$180x10^4$ ECL counts, respectively). Currently, what causes the increase in ECL signal is unclear and, therefore, one should be careful when interpreting ECL data if such an increase in signal is observed. However, the similarities between the ECL counts observed in the case of deoxycholic acid and the randomized ssDNA suggest that the presence of deoxycholic acid might unfold the aptamer structure. Such unfolding would bring the $Ru(bpy)_3^{2+}$ labels further away from the electrode surface

and closer to the light source, leading to a higher number of counts as was previously discussed in section 3.2. [43]. This hypothesis would be supported by the shift of charge states towards more positive charges (i.e. the peak of the 8+ charge state) observed during the native nESI-MS experiments (**Fig. 4f**) which usually means a more unfolded structure due to a larger solvent-accessible surface being presented [7]. Furthermore, it is important to highlight herein that deoxycholic acid and its sodium form are used as biosurfactants in biological research for membrane solubilization, reconstitution of proteins and so forth [44,45]. It is reported that when interacting with proteins it promotes a major denaturation (unfolding) and loss of their structure [46]. Hence, the deoxycholic acid seems to somehow disrupt the structural conformation of TESS.1 at higher concentrations (**Fig. 4e**) which could promote the unfolding of the aptamer, with similar results as the randomized sequence (**Fig. 4d**), rather than complexation (0% of complex formation, **Fig. 4f**).

Finally, the addition of increasing concentrations of hydrocortisone to the TESS.1 aptamer first leads to a small increase of the ECL signal but afterward decreases up to 31% of its initial value (**Fig. 4g,** inset). It is important to remark that the trend of this last part is similar to the one of the binding of testosterone to the TESS.1 aptamer, but with less intensity difference indicating only low-affinity binding. This is also supported by native nESI-MS data in which a small amount of complex (19%) between the TESS.1 aptamer and hydrocortisone was detected (**Fig. 4h**).

4. Conclusions

A novel ECL assay based on aptamer recognition towards testosterone, as a model for small molecules, was introduced. This proof of concept study can be extended towards other steroids and small molecules in the future. Inspired by the binding competent principle published by Yang and coworkers, the system consisting of a capture probe, aptamer and target was characterized using a multifaceted approach with analytical techniques such as ITC and native nESI-MS. The stems of the TESS.1 aptamer were found to play a crucial role in the binding mechanism since they hybridize upon binding of testosterone. Therefore, stem 1 can no longer interact with the capture probe and the aptamer-capture probe interaction was disrupted while an aptamer-testosterone complex was formed.

Knowing the working mechanism of the system, a reliable ECL assay was developed for the detection of testosterone. The ECL assay could detect testosterone with a linear range from 0.39 to 1.56 µM and a limit of detection of 0.29 µM. Furthermore, the assay was found to be selective and specific since testosterone does not bind to a randomized DNA sequence and the aptamer does not respond to deoxycholic acid and only weakly to hydrocortisone. Although aptamer-based ECL sensors emerged only over one decade ago, they have already found broad applications in both fundamental research and biomedical diagnostics applications.

The present work aims to open a new avenue for the development of reliable and robust ECL biosensor assays for biochemical analysis, promoting a deeper

understanding of the potential of biosensors based on aptamers for the accurate detection of numerous biomolecules relevant in biomedical applications.

Declaration of competing interest

The authors declare that they have no known competing financial interests or personal relationships that could have appeared to influence the work reported in this paper.

CRediT authorship contribution statement

Rocío Cánovas: Conceptualization, Data curation, Formal analysis, Investigation, Methodology, Validation, Visualization, Writing - original draft; Writing - review & editing. **Elise Daems**: Conceptualization, Data curation, Formal analysis, Investigation, Methodology, Validation, Visualization, Writing - original draft; Writing - review & editing. **Rui Campos**: Conceptualization, Data curation, Investigation, Methodology, Validation, Writing - original draft; Writing - review & editing. **Sofie Schellinck**: Conceptualization, Writing - review & editing. **Annemieke Madder**: Conceptualization, Funding acquisition, Supervision, Writing - review & editing. **José C. Martins:** Conceptualization, Funding acquisition, Supervision, Writing - review & editing. **Frank Sobott:** Resources, Writing - review & editing. **Karolien De Wael**: Conceptualization, Investigation, Funding acquisition, Project administration, Resources, Supervision, Writing - review & editing.

Acknowledgments and funding sources

The authors would like to acknowledge the financial support from FWO (Research Foundation – Flanders) grant number 1S65717N, 2017 and G054819N, 2018, Rui Campos and Rocío Cánovas would like to acknowledge the funding received from the European Union's Horizon 2020 research and innovation program under the Marie Skłodowska-Curie grant agreement No 842219 and 101024231, respectively. Furthermore, the authors acknowledge Dr. Deborah Decrop, from MSD, for her help with the MSD quickplex instrument and MSD for lending us the equipment and Dr. Pieter Van Wielendaele for his assistance during the ITC measurements. Finally, we would also like to acknowledge Prof. Dr. Peter Vandenabeele for allowing us to use the MSD quickplex instrument at VIB-UGENT and Dr. Peter Tougaard for assisting in some measurements.

References

[1] M. Prante, E. Segal, T. Scheper, J. Bahnemann, J. Walter, Aptasensors for Point-of-Care Detection of Small Molecules, Biosensors. 108 (2020) 1–19.

[2] G.S. Yadav, V. Kumar, N.K. Aggarwal, Aptamers: Biotechnological applications of a next generation tool, 2019. https://doi.org/10.1007/978-981-13-8836-1.

[3] W.-W. Zhao, J.-J. Xu, H.-Y. Chen, Photoelectrochemical aptasensing, TrAC - Trends Anal. Chem. 82 (2016) 307–315. https://doi.org/10.1016/j.trac.2016.06.020.

[4] Y.N. Khonsari, S. Sun, Recent trends in electrochemiluminescence

aptasensors and their applications, Chem. Commun. 53 (2017) 9042–9054. https://doi.org/10.1039/c7cc04300g.

[5] K.A. Yang, H. Chun, Y. Zhang, S. Pecic, N. Nakatsuka, A.M. Andrews, T.S. Worgall, M.N. Stojanovic, High-Affinity Nucleic-Acid-Based Receptors for Steroids, ACS Chem. Biol. 12 (2017) 3103–3112. https://doi.org/10.1021/acschembio.7b00634.

[6] F. Melaine, C. Coilhac, Y. Roupioz, A. Buhot, A nanoparticle-based thermo-dynamic aptasensor for small molecule detection, Nanoscale. 8 (2016) 16947–16954. https://doi.org/10.1039/c6nr04868d.

[7] E. Daems, D. Dewaele, K. Barylyuk, K. De Wael, F. Sobott, Aptamer-ligand recognition studied by native ion mobility-mass spectrometry, Talanta. 224 (2021) 121917. https://doi.org/10.1016/j.talanta.2020.121917.

[8] Y. Zhao, K. Yavari, J. Liu, Critical evaluation of aptamer binding for biosensor designs, TrAC Trends Anal. Chem. (2021) 116480. https://doi.org/10.1016/j.trac.2021.116480.

[9] F. Bottari, E. Daems, A.M. de Vries, P. Van Wielendaele, S. Trashin, R. Blust, F. Sobott, A. Madder, J.C. Martins, K. De Wael, Do Aptamers Always Bind? The Need for a Multifaceted Analytical Approach When Demonstrating Binding Affinity between Aptamer and Low Molecular Weight Compounds, J. Am. Chem. Soc. 142 (2020) 19622–19630. https://doi.org/10.1021/jacs.0c08691.

[10] E. Daems, G. Moro, R. Campos, K. De Wael, Mapping the gaps in chemical analysis for the characterisation of aptamer-target interactions, TrAC - Trends Anal. Chem. 142 (2021) 116311. https://doi.org/10.1016/j.trac.2021.116311.

[11] K. Ikebukuro, C. Kiyohara, K. Sode, Electrochemical Detection of Protein Using a Double Aptamer Sandwich, Anal. Lett. 37 (2004) 2901–2909. https://doi.org/10.1081/AL-200035778.

[12] H. Liu, Y. Xiang, Y. Lu, R.M. Crooks, Aptamer-Based Origami Paper Analytical Device for Electrochemical Detection of Adenosine, Angewandte. 124 (2012) 7031–7034. https://doi.org/10.1002/ange.201202929.

[13] Q. Liu, Y. Peng, J. Xu, C. Ma, L. Li, C. Mao, J.-J. Zhu, Label-Free Electrochemiluminescence Aptasensor for Highly Sensitive Detection of Acetylcholinesterase Based on Au-Nanoparticle-Functionalized g-C3N4 Nanohybrid, ChemElectroChem. 4 (2017) 1768–1774. https://doi.org/10.1002/celc.201700035.

[14] Y.N. Khonsari, S. Sun, A novel label free electrochemiluminescent aptasensor for the detection of lysozyme, Mater. Sci. Eng. C. 96 (2019) 146–152. https://doi.org/10.1016/j.msec.2018.11.016.

[15] J. Pultar, U. Sauer, P. Domnanich, C. Preininger, Aptamer–antibody on-chip sandwich immunoassay for detection of CRP in spiked serum, Biosens. Bioelectron. 24 (2009) 1456–1461. https://doi.org/10.1016/j.bios.2008.08.052.

[16] O.A. Alsager, S. Kumar, J.M. Hodgkiss, Lateral Flow Aptasensor for Small Molecule Targets Exploiting Adsorption and Desorption Interactions on Gold Nanoparticles, Anal. Chem. 89 (2017) 7416–7424.

https://doi.org/10.1021/acs.analchem.7b00906.

[17] A. Nezami, R. Nosrati, B. Golichenari, R. Rezaee, G.I. Chatzidakis, A.M. Tsatsakis, G. Karimi, Nanomaterial-based aptasensors and bioaffinity sensors for quantitative detection of 17β-estradiol, TrAC - Trends Anal. Chem. 94 (2017) 95–105. https://doi.org/10.1016/j.trac.2017.07.003.

[18] V. Skouridou, M. Jauset-rubio, P. Ballester, A.S. Bashammakh, M.S. El-shahawi, A.O. Alyoubi, C.K. O'Sullivan, Selection and characterization of DNA aptamers against the steroid testosterone, Microchim. Acta. 184 (2017) 1631–1639. https://doi.org/10.1007/s00604-017-2136-0.

[19] J. Wang, J. Hou, H. Zhang, Y. Tian, L. Jiang, Single Nanochannel-Aptamer-Based Biosensor for Ultrasensitive and Selective Cocaine Detection, Appl. Mater. Interfaces. 10 (2018) 2033–2039. https://doi.org/10.1021/acsami.7b16539.

[20] M.Y. Ho, N. D'Souza, P. Migliorato, Electrochemical Aptamer-Based Sandwich Assays for the Detection of Explosives, Anal. Chem. 84 (2012) 4245–4247. https://doi.org/10.1021/ac300606n.

[21] K. Han, T. Liu, Y. Wang, P. Miao, Electrochemical aptasensors for detection of small molecules, macromolecules, and cells, Rev. Anal. Chem. 35 (2016) 201–211. https://doi.org/10.1515/revac-2016-0009.

[22] E. Farjami, R. Campos, J.S. Nielsen, K. V. Gothelf, J. Kjems, E.E. Ferapontova, RNA aptamer-based electrochemical biosensor for selective and label-free analysis of dopamine, Anal. Chem. 85 (2013) 121–128. https://doi.org/10.1021/ac302134s.

[23] B. Babamiri, D. Bahari, A. Salimi, Highly sensitive bioaffinity electrochemiluminescence sensors: Recent advances and future directions, Biosens. Bioelectron. 142 (2019) 111530. https://doi.org/10.1016/j.bios.2019.111530.

[24] C. Ma, Y. Cao, X. Gou, J.-J. Zhu, Recent progress in electrochemiluminescence sensing and imaging, Anal. Chem. 92 (2020) 431–454. https://doi.org/10.1021/acs.analchem.9b04947.

[25] J. Duo, C. Chiriac, R.Y.-C. Huang, J. Mehl, G. Chen, A. Tymiak, P. Sabbatini, R. Pillutla, Y. Zhang, Slow Off-Rate Modified Aptamer (SOMAmer) as a Novel Reagent in Immunoassay Development for Accurate Soluble Glypican-3 Quantification in Clinical Samples, Anal. Chem. 90 (2018) 5162–5170. https://doi.org/10.1021/acs.analchem.7b05277.

[26] X. Feng, N. Gan, H. Zhang, Q. Yan, T. Li, Y. Cao, F. Hu, H. Yu, Q. Jiang, A novel "dual-potential" electrochemiluminescence aptasensor array using CdS quantum dots and luminol-gold nanoparticles as labels for simultaneous detection of malachite green and chloramphenicol, Biosens. Bioelectron. 74 (2015) 587–593. https://doi.org/10.1016/j.bios.2015.06.048.

[27] H. Shi, M. Wu, Y. Du, J. Xu, H. Chen, Electrochemiluminescence aptasensor based on bipolar electrode for detection of adenosine in cancer cells, Biosens. Bioelectron. 55 (2014) 459–463. https://doi.org/10.1016/j.bios.2013.12.045.

[28] H. Zhang, F. Luo, P. Wang, L. Guo, B. Qiu, Z. Lin, Signal-on electrochemiluminescence aptasensor for bisphenol A based on hybridization chain reaction and electrically heated electrode, Biosens. Bioelectron. 129 (2019) 36–41. https://doi.org/10.1016/j.bios.2019.01.007.

[29] Y. Yu, Q. Cao, M. Zhou, H. Cui, A novel homogeneous label-free aptasensor for 2,4,6-trinitrotoluene detection based on an assembly strategy of electrochemiluminescent graphene oxide with gold nanoparticles and aptamer, Biosens. Bioelectron. 43 (2013) 137–142. https://doi.org/10.1016/j.bios.2012.12.018.

[30] S. Cheng, H. Liu, H. Zhang, G. Chu, Y. Guo, X. Sun, Ultrasensitive electrochemiluminescence aptasensor for kanamycin detection based on silver nanoparticle-catalyzed chemiluminescent reaction between luminol and hydrogen peroxide, Sensors Actuators B. Chem. 304 (2020) 127367. https://doi.org/10.1016/j.snb.2019.127367.

[31] S. Cheng, H. Zhang, J. Huang, R. Xu, X. Sun, Y. Guo, Highly sensitive electrochemiluminescence aptasensor based on dual-signal ampli fi cation strategy for kanamycin detection, Sci. Total Environ. 737 (2020) 139785. https://doi.org/10.1016/j.scitotenv.2020.139785.

[32] X. Liu, L. Luo, L. Li, Z. Di, J. Zhang, T. You, An electrochemiluminescence aptasensor for analysis of bisphenol A þ based on carbon nanodots composite as co-reaction of Ru (bpy)32+ nanosheets, Electrochim. Acta. 319 (2019) 849–858. https://doi.org/10.1016/j.electacta.2019.07.035.

[33] M. Wei, C. Wang, E. Xu, J. Chen, X. Xu, W. Wei, S. Liu, A simple and sensitive electrochemiluminescence aptasensor for determination of ochratoxin A based on a nicking endonuclease-powered DNA walking machine, Food Chem. 282 (2019) 141–146. https://doi.org/10.1016/j.foodchem.2019.01.011.

[34] L. Luo, S. Ma, L. Li, X. Liu, J. Zhang, X. Li, D. Liu, T. You, Monitoring zearalenone in corn flour utilizing novel self-enhanced electrochemiluminescence aptasensor based on NGQDs-NH2-Ru@SiO2 luminophore, Food Chem. 292 (2019) 98–105. https://doi.org/10.1016/j.foodchem.2019.04.050.

[35] H. Xiong, J. Gao, Y. Wang, Z. Chen, M.-M. Chen, X. Zhang, S. Wang, Construction of Ultrasensitive Electrochemiluminescent Aptasensor for Ractopamine Detection, Analist. 00 (2019) 1–6. https://doi.org/10.1039/C9AN00183B.

[36] K. Lin, G. Wu, Chapter 19 Isothermal Titration Calorimetry Assays to Measure Binding Affinities In Vitro, in: Hippo Pathway. Methods Mol. Biol., Humana Press, New York, NY, 2019: pp. 257–272. https://doi.org/https://doi.org/10.1007/978-1-4939-8910-2_19.

[37] A.C. Leney, A.J.R. Heck, Native Mass Spectrometry: What is in the Name?, J. Am. Soc. Mass Spectrom. 28 (2017) 5–13. https://doi.org/10.1007/s13361-016-1545-3.

[38] ® MESO SCALE DISCOVERY, Meso Scale Discovery (MSD®) Labeling

Reagents: MSD GOLD SULFO-TAG NHS-Ester, 2018.

[39] W. Miao, Electrogenerated chemiluminescence and its biorelated applications, Chem. Rev. 108 (2008) 2506–2553. https://doi.org/10.1021/cr068083a.

[40] A. Decarie, G. Drapeau, J. Closset, R. Couture, A. Adams, Development of Digoxigenin-Labeled Peptide: Application to Chemiluminoenzyme Immunoassay of Bradykinin in Inflamed Tissues, Peptides. 15 (1994) 511–518. https://doi.org/10.1016/0196-9781(94)90214-3.

[41] T. Sakamoto, E. Ennifar, Y. Nakamura, Thermodynamic study of aptamers binding to their target proteins, Biochimie. 145 (2018) 91–97. https://doi.org/10.1016/j.biochi.2017.10.010.

[42] J.R. Chambers, K. Sauer, Detection of cyclic di-GMP binding proteins utilizing a biotinylated cyclic di-GMP pulldown assay Jacob, Methods Mol Biol. 1657 (2017) 139–148. https://doi.org/10.1007/978-1-4939-7240-1_25.

[43] M. Wang, Y. Zhou, H. Yin, W. Jiang, H. Wang, S. Ai, Signal-on electrochemiluminescence biosensor for microRNA-319a detection based on two-stage isothermal strand-displacement polymerase reaction, Biosens. Bioelectron. 107 (2018) 34–39. https://doi.org/10.1016/j.bios.2018.02.015.

[44] J.M. Neugebauer, Detergents: An overview, Methods Enzymol. 182 (1990) 239–253. https://doi.org/10.1016/0076-6879(90)82020-3.

[45] A. Helenius, K. Simons, Solubilization of membranes by detergents, Biochim. Biophys. Acta. 415 (1975) 29–79.

[46] B.K. Paul, R. Sett, N. Guchhait, Stepwise unfolding of Ribonuclease A by a biosurfactant, J. Colloid Interface Sci. 505 (2017) 673–681. https://doi.org/10.1016/j.jcis.2017.06.051.